MOVING GRID NUMERICAL SIMULATIONS OF PLANAR TIME-DEPENDENT DETONATIONS

Longting HE[1] and Bernard LARROUTUROU[2]

Abstract

We present an efficient and accurate numerical method for the accurate solution of one-dimensional time-dependent detonation problems. The numerical method combines an upwind shock capturing method of TVD type with a moving grid method. This combination, although simple, allows us to perfectly capture the Neumann spike of the detonation front. Several numerical examples are given that show the ability of the developed numerical schemes to accurately solve time-dependent detonation problems, including the "galloping" detonations instabilities, with simple chemistry or with a realistic hydrogen-oxygen chemical mechanism.

SIMULATIONS NUMERIQUES SUR MAILLAGES MOBILES DE DETONATIONS PLANES INSTATIONNAIRES

Résumé

Pour le calcul d'ondes de détonations planes instationnaires, nous présentons une méthode combinant un schéma décentré de type TVD et une technique de maillage mobile. Cette méthode simple permet de capturer parfaitement le pic de pression de Von Neumann dans le front de détonation. Plusieurs résultats sont présentés, montrant notamment les instabilités "galopantes" de front de détonations, avec une chimie simple ou avec un mécanisme chimique réaliste pour la combustion hydrogène-oxygène.

[1]Laboratoire de Recherche en Combustion, URA CNRS 1117 and Université de Provence, Centre Saint Jérôme, 13397 Marseille CEDEX 13

[2]CERMICS, INRIA, B.P. 93, 06902 Sophia–Antipolis Cedex, France, and Ecole Polytechnique, 91128 Palaiseau Cedex, France

1 INTRODUCTION

The structure of a steady detonation wave, which consists of a shock wave travelling at supersonic velocity followed by a reaction zone [11, 32, 36], is easily described analytically. Through the forward inert shock wave, the mixture is compressed and heated to the so-called Neumann state, and chemical reaction then begins in the heated gas; as the reaction proceeds, heat is released, pressure and density decrease, and this process goes on until the combustion is complete. These steady ZND (Zeldovich-Neumann-Döring) detonations waves are very different from reaction-diffusion *flames*, in particular because the chemical reaction rates and above all the molecular transports effects have little influence on the speed of the propagating wave.

However, the behaviour of the time-dependent detonations, such as their instabilities and their initiation, are difficult to describe analytically: they strongly depend on the interaction between the chemical reactions and gas dynamics. A full understanding of these time-dependent phenomena requires reliable and highly accurate numerical simulations of this coupled phenomena.

The main difficulties of the numerical simulations of time-dependent detonations are related to the spatial stiffness due to disparate length scales and to the inaccurate representation of the Neumann spike due to the inherent artificial diffusion of the numerical method. In contrast with nonreactive compressible flows, reactive flows involving detonations have an intrinsic length scale, the so-called chemical reaction length which is approximately given as the product of the characteristic chemical reaction time multiplied by the characteristic flow velocity. This reaction length typically ranges between 10^{-5} m and 10^{-2} m, which may be 10^5 times smaller than the characteristic length of the practical problem. In order to accurately treat the interaction between the chemical reactions and the gas dynamics, the numerical resolution scale (i.e., the mesh size) must be smaller than the chemical reaction length scale. Using different methods, Colella *et al.* [8], Ben-Artzi [2], LeVeque and Yee [25] have reported that non physical results can be obtained for steady detonation propagations when the mesh size is larger than the reaction length. This type of spatial stiffness problem may be easily resolved for some problems, such as the galloping detonations instabilities, because a computational domain of the order of ten reaction lengths moving with the front is sufficient to represent this phenomenon, and a uniform spatial discretization may be used adequately. The situation is completely different for the initiation of detonations: the length scale of the development of detonations is in general of the order of magnitude of 10^4 reaction lengths, so that an adaptive mesh strategy *must* be used.

Many efficient shock capturing numerical methods have recently been developed for computing *non reactive* compressible flows. The methods currently in use are the Total-Variation-Diminishing (TVD) method [10, 15, 33, 34], the Essentially-Non-Oscillatory (ENO) method [16], the Flux-Corrected-Transport (FCT) method [3, 27], the Piecewise-Parabolic method (PPM) [9], the MUSCL method [31] and the Random-Choice method (RCM) [7]. These methods can be made second-order accurate or even higher-order accurate in space and oscillation-free across discontinuities. However all these methods except RCM capture the shock wave over three or four mesh points. When these methods are extended directly to reactive flows containing detonations, the captured Neumann spike is then smeared; as a consequence, since the chemical induction time strongly depends on the temperature, the inaccurate representation of the Neumann state introduces important numerical errors. In particular, when a detailed chemistry is considered, inaccurate representation of the Neumann state may shorten very much the chem-

ical induction time due to the presence of radicals in the mixture at the Neumann state. The numerical solution may of course be improved at the Neumann spike by increasing the spatial resolution, but this makes the algorithm inefficient.

It is therefore crucial to reduce the numerical viscosity at the leading shock of a detonation wave. In [4, 5], this goal was achieved by using a numerical method combining the PPM method, the shock-tracking method of Chern and Collela [6] and a grid refinement strategy. In [18], the first author used a TVD upwind method combined with a conservative variant of the shock tracking method of Mao [26]; this method has been used for the simulation of galloping detonation instabilities, and of detonation initiations [19]. Notice that these two series of works [4, 5] and [18, 19] use a *fixed* computational grid.

In this paper, we propose a simpler numerical method for the high resolution of time-dependent detonation problems. This goal is achieved by incorporating moving grid methods to an upwind TVD approximation; no shock tracking algorithm is employed. The advantage of our method is its simplicity and its accuracy. The numerical results presented below show indeed that the developed algorithms very accurately simulate time-dependent detonations. In particular, we will simulate the galloping detonation instabilities with a realistic chemical mechanism for hydrogen combustion; to the best of our knowledge, this numerical experiment is the very first simulation of detonations involving complex chemistry.

The outline of the paper is as follows: the governing equations are described in Section 2, whereas we describe the numerical methods in Section 3 and discuss the numerical results in Section 4.

2 GOVERNING EQUATIONS

For the sake of simplicity, we present here the governing equations in the case of a single one-step reaction $A \longrightarrow B$, with constant specific heats. Neglecting the molecular transport effects, the conservation equations for mass, momentum and energy in planar geometry are written as:

$$\frac{\partial W}{\partial t} + \frac{\partial F(W)}{\partial x} = \Omega(W) \ , \tag{1}$$

with:

$$\begin{aligned} W &= (\rho Y_1, \rho Y_2, \rho u, E)^T \ , \\ F(W) &= \left(\rho u Y_1, \rho u Y_2, \rho u^2 + p, u(E+p)\right)^T \ , \\ \Omega(W) &= (-\omega, \omega, 0, 0)^T \ . \end{aligned} \tag{2}$$

The ideal gas law is written as:

$$p = \rho T \ , \tag{3}$$

and the total energy E is given by:

$$E = \rho \left(\frac{T}{\gamma - 1} + Q Y_1 + \frac{1}{2} u^2 \right) \ . \tag{4}$$

The consumption mass rate of the reactant A is modelled using the law of mass action and the Arrhenius law:

$$\omega = B \rho Y_1 \exp\left(-\frac{\beta}{T}\right) \ . \tag{5}$$

In these relations, ρ, p, T, Y_1 and Y_2 respectively denote the normalised density, pressure, temperature, total energy of the mixture and the reactant and product mass fractions. The normalisation involves a reference state, which will be specified in the numerical examples below. In particular, the velocity u is normalised using the sound speed c at the reference state divided by the square root of the specific heats ratio γ. The reference time $t_{1/2}$ is the time needed for a fluid particle to travel from the leading shock to a position where $Y_1 = 0.5$. The reference length scale is thus $L_{1/2} = \dfrac{t_{1/2}c}{\sqrt{\gamma}}$, which is typically of the same order as the thickness of the detonation front.

The other dimensionless parameters appearing in (4)-(5) are the specific heats ratio γ, the chemical heat release Q and the normalised activation energy β. Let us recall that the propagation speed D_{CJ} and the structure of a steady CJ detonation are fully determined by these three dimensionless parameters, and that the degree of overdrive of a strong detonation travelling with speed D is measured by the parameter $f = \left(\dfrac{D}{D_{CJ}}\right)^2 > 1$ [13].

3 NUMERICAL METHODS

Let us now describe the numerical methods. Following [5, 8], we use a time splitting method to treat separately the chemical reaction process and the hydrodynamical process. The ordinary differential equations describing the chemical reaction are integrated implicitly. The emphasis is put in the description below on the resolution of the generalised Euler equations.

3.1 Time splitting scheme

Since the chemical reaction rate depends strongly on temperature, it is in general needed to resolve the chemical reaction term implicitly. In order to avoid costly matrix operations and to use the best (i.e., the least dissipative) method for the hyperbolic equations, we employ a time splitting scheme, in which the chemical reaction process and hydrodynamical process are solved independently. We write:

$$W^{n+1} = \mathcal{L}_c^{\Delta t/2}\ \mathcal{L}_f^{\Delta t}\ \mathcal{L}_c^{\Delta t/2}\ W^n\ , \tag{6}$$

where the operator $\mathcal{L}_c^{\Delta t/2}$ represents the numerical solution of the purely chemical reactions process

$$\frac{\partial W}{\partial t} = \Omega(W) \tag{7}$$

over a half time step, and the operator $\mathcal{L}_f^{\Delta t}$ represents the numerical solution for the hyperbolic equations

$$\frac{\partial W}{\partial t} + \frac{\partial F(W)}{\partial x} = 0 \tag{8}$$

for the fluid motion over a complete time step Δt.

Physically, the chemical process is a purely local constant-density evolution during which temperature and pressure are both increased; whereas the fluid part (8) of the equations involve the interaction between neighbouring cells. We now present the moving grid method used to solve the latter.

3.2 Roe's method on a moving grid

The generalised Euler equations (8) for a two-component mixture are known to be hyperbolic (see e.g. [22]), which allows us to use one of the available Godunov-type methods for the solutions of this system. Among these methods, we choose here Roe's method because of its ability to perfectly resolve shocks, as we will see later. Actually, we will use Roe's method operating on a moving grid, as was done by Harten and Hyman [17] for single-component shock-tubes. The extension to second-order accuracy will be done using the upwind TVD formulation developed by Harten and Yee (see e.g. [15, 35]).

3.2.1 The moving grid formulation

Let us consider a set of moving mesh points $\left[X_1^n, X_2^n, \cdots, X_j^n, \cdots, X_J^n\right]$, separated by moving cell interfaces $\left[\xi_{3/2}^n, \cdots, \xi_{j+1/2}^n, \cdots, \xi_{J-1/2}^n\right]$, as shown on Figure 1; the superscript n denotes the n^{th} time level. Initially, we take the midpoint of the X_j's as the interfaces: $\xi_{j+1/2}^0 = \dfrac{X_j^0 + X_{j+1}^0}{2}$.

An explicit conservative scheme for the fluid system (8) on this variable mesh takes the form (see e.g. [17]):

$$\left(\xi_{j+1/2}^{n+1} - \xi_{j-1/2}^{n+1}\right) W_j^{n+1} - \left(\xi_{j+1/2}^n - \xi_{j-1/2}^n\right) W_j^n + \Delta t^n \left(\mathcal{F}_{j+1/2}^n - \mathcal{F}_{j-1/2}^n\right) = 0 \ . \tag{9}$$

As usual, the Roe fluxes $\mathcal{F}_{j+1/2}^n$ are based on a linearisation of the flux function $F(W)$. They can be obtained by writing a Godunov-type formulation on the trapezoidal space-time cells of Figure 1, or equivallently by writing the usual (fixed-grid) fluxes for the following linearized system written in grid-attached coordinates:

$$\frac{\partial W}{\partial t} + \left(\tilde{A}_{j+1/2}^n - \dot{\xi}_{j+1/2}^n\right) \frac{\partial W}{\partial x} = 0 \ ; \tag{10}$$

here, $\tilde{A}_{j+1/2}^n = \tilde{A}\left(W_j^n, W_{j+1}^n\right)$ is the multi-component Roe matrix of the states W_j^n and W_{j+1}^n, which satisfies the Roe relation:

$$\tilde{A}\left(W_j^n, W_{j+1}^n\right)\left(W_{j+1}^n - W_j^n\right) = F\left(W_{j+1}^n\right) - F\left(W_j^n\right) \ , \tag{11}$$

and $\dot{\xi}_{j+1/2}^n = \dfrac{\xi_{j+1/2}^{n+1} - \xi_{j+1/2}^n}{\Delta t^n}$ is the speed of the moving interface. The matrix $\tilde{A}$ has four eigenvalues:

$$\lambda_1 = \tilde{u} - \tilde{c} \ , \quad \lambda_2 = \lambda_3 = \tilde{u} \ , \quad \lambda_4 = \tilde{u} + \tilde{c} \ , \tag{12}$$

where $\tilde{c}$ is the frozen sound velocity, and a complete set of real right eigenvectors; we denote $\tilde{R}$ the matrix whose collumns are these right eigenvectors of $\tilde{A}$. With these notations, the flux $\mathcal{F}_{j+1/2}^n$ writes:

$$\mathcal{F}_{j+1/2}^n = \frac{1}{2}\left[\left(F(W_j^n) - \dot{\xi}_{j+1/2}^n W_j^n\right) + \left(F(W_{j+1}^n) - \dot{\xi}_{j+1/2}^n W_{j+1}^n\right) + \tilde{R}_{j+1/2}^n \Phi_{j+1/2}^n\right] \ , \tag{13}$$

with:

$$\Phi^n_{j+1/2} = \sum_{k=1}^{4} \Psi\left(\lambda_k - \dot{\xi}^n_{j+1/2}\right)\left(\alpha^n_{j+1/2}\right)_k \ , \tag{14}$$

$$\Psi(z) = \begin{cases} |z| & \text{if } |z| \geq \delta \ , \\ \dfrac{z^2+\delta^2}{2\delta} & \text{if } |z| \leq \delta \ , \end{cases} \tag{15}$$

$$\alpha^n_{j+1/2} = \left(\tilde{R}^n_{j+1/2}\right)^{-1}\left(W^n_{j+1} - W^n_j\right) \ . \tag{16}$$

In (15), we have used Harten's correction [14] in order to avoid entropy-violating shocks.

The moving-grid second-order accurate upwind TVD extension of this scheme consists in modifying the vector $\Phi^n_{j+1/2}$ as follows in the above expressions:

$$\Phi^n_{j+1/2} = \sum_{k=1}^{4} \sigma^n_{j+1/2}\left(\lambda_k - \dot{\xi}^n_{j+1/2}\right)\left(\frac{(G_j)_k + (G_{j+1})_k}{2}\right) - \Psi\left(\lambda_k - \dot{\xi}^n_{j+1/2} + (\gamma_{j+1/2})_k\right)\left(\alpha^n_{j+1/2}\right)_k \ , \tag{17}$$

with:

$$\sigma^n_{j+1/2}(z) = \Psi(z) - \frac{2\Delta t^n}{\xi^n_{j+3/2} - \xi^n_{j-1/2}} z^2 \ , \tag{18}$$

$$(\gamma_{j+1/2})_k = \sigma^n_{j+1/2}\left(\lambda_k - \dot{\xi}^n_{j+1/2}\right) \times \begin{cases} \dfrac{(G_{j+1})_k - (G_j)_k}{(\alpha^n_{j+1/2})_k} & \text{if } (\alpha^n_{j+1/2})_k \neq 0 \ , \\ 0 & \text{if } (\alpha^n_{j+1/2})_k = 0 \ , \end{cases} \tag{19}$$

$$(G_j)_k = S \ \max\left[0, \ \min\left(2|(\alpha^n_{j+1/2})_k|, S(\alpha^n_{j-1/2})_k\right), \ \min\left(|(\alpha^n_{j+1/2})_k|, 2S(\alpha^n_{j-1/2})_k\right)\right] \ . \tag{20}$$

In the relation (20) which involves Roe's superbee limiter [29], we used the notation $S = sign\left((\alpha^n_{j+1/2})_k\right)$.

3.2.2 Moving grid strategies

It remains to define how to move the grid points. We will consider two simple moving grid strategies. For the sake of simplicity, we now describe these two strategies for the particular case of a solution to system (8) which involves only one shock wave propagating with speed s; this description will be adequate since our aim is to simulate planar detonation waves, which contain only one leading shock wave. Let us then temporarily assume that our initial data simply is:

$$W^0_j = \begin{cases} W_L & \text{if } j \leq j_0 \ , \\ W_R & \text{if } j > j_0 \ , \end{cases} \tag{21}$$

for some integer j_0, the two states W_L and W_R satisfying:

$$F(W_R) - F(W_L) = s(W_R - W_L) \ . \tag{22}$$

A first simple method, which we will simply call the moving grid (MG) method, consists in moving a fixed number of grid points around the shock with the shock speed. If the shock

is located at the interface $\xi^n_{k+1/2}$ at the n^{th} time level, then the shock speed $s^n_{k+1/2}$ is determined by the Roe method (for instance, it is easy to see from (11), (21), (22) that $s^0_{j_0+1/2} = s$ is an eigenvalue of the Roe matrix $\tilde{A}^0_{j_0+1/2}$). Thus, we make $(N_l + N_r + 1)$ mesh points $[X_{k-N_l}, X_{k-N_l+1}, \cdots, X_k, \cdots, X_{k+N_r}]$ and $(N_l + N_r + 2)$ cell interfaces move with the shock (see Figure 2 for $N_l = N_r = 1$):

$$\begin{cases} X^{n+1}_j = X^n_j + s^n_{k+1/2}\Delta t^n & \text{for } k - N_l \le j \le k + N_r \ , \\ \xi^{n+1}_{j+1/2} = \xi^n_{j+1/2} + s^n_{k+1/2}\Delta t^n & \text{for } k - N_l - 1 \le j \le k + N_r \ . \end{cases} \tag{23}$$

In order to avoid the collision of mesh points, or to avoid the formation of very small cells, we examine at each time level the smallest mesh size. Assuming that $s^n_{k+1/2} > 0$ for the sake of clarity, we eliminate the mesh point X_{k+N_r+1} and add a new mesh point between X_{k-N_l-1} and X_{k-N_l} if $X_{k+N_r-1} - X_{k+N_r} < \dfrac{\Delta x}{2}$ (Δx is the initial mesh spacing). In this way, if N_l and N_r are large enough, the pertubations due to projection and interpolation occur far away from the shock wave; we use a conservative interpolation [21].

Our second moving mesh strategy is very close to the self-adjusting grid (SAG) method proposed by Harten and Hyman [17]. In this method, the mesh points X_j are kept fixed, and the speed of the moving cell interfaces is chosen so that the location of the shock coincides with one of the interfaces. Still assuming for the sake of clarity that the shock is located at the interface $\xi^n_{k+1/2}$ at the n^{th} time level and moves with the speed $s^n_{k+1/2} \ge 0$, we call $\xi^{n+1}_{shock} = \xi^n_{k+1/2} + s^n_{k+1/2}\Delta t^n$ the new shock position; the motion of the interfaces is then determined as follows:

(a) If the new shock location stays in the k^{th} interval, i.e. if $X_k < \xi^{n+1}_{shock} < X_{k+1}$, then:

$$\xi^{n+1}_{k+1/2} = \xi^{n+1}_{shock} \ , \quad \xi^{n+1}_{j+1/2} = \xi^n_{j+1/2} \quad \text{for } j \ne k \ . \tag{24}$$

(b) If the shock is located in the next interval at time t^{n+1}, i.e. if $X_{k+1} \le \xi^{n+1}_{shock} < X_{k+2}$, then:

$$\xi^{n+1}_{k+1/2} = \frac{X_k + X_{k+1}}{2} \ , \quad \xi^{n+1}_{k+3/2} = \xi^{n+1}_{shock} \ , \quad \xi^{n+1}_{j+1/2} = \xi^n_{j+1/2} \quad \text{for } j \ne k, k+1 \ . \tag{25}$$

These two cases are shown on Figure 3. Notice that the distinction between cases *(a)* and *(b)* allows us to avoid too small cells. Also, case *(a)* is equivallent to the previous MG method with $N_l = N_r = 0$.

It is a simple exercice on the Roe and Rankine-Hugoniot relations (11) and (22) to prove that, for the simple case (21)-(22), *both MG and SAG methods provide the exact solution*, that is:

$$\xi^n_{shock} = \xi^0_{j_0+1/2} + st^n \quad \text{for all } n \ge 0 \ , \tag{26}$$

$$W^n_j = \begin{cases} W_L & \text{if } X^n_j \le \xi^n_{shock} \ , \\ W_R & \text{if } X^n_j > \xi^n_{shock} \ . \end{cases} \tag{27}$$

Notice that these properties remain true even with case *(b)* of Figure 3, where no interface is actually following the shock path, but where the shock location still coincides at each time level with a cell interface.

In view of this property, since the planar detonation waves contain only one leading shock wave, we expect to resolve perfectly this leading shock for the detonation problems using these two moving grid strategies. It is precisely the objective of the next section to examine how these methods behave and to compare the MG and SAG strategies.

4 NUMERICAL RESULTS

We now present some numerical results, obtained with the second-order accurate TVD Roe scheme described above. Our test problems include an inert flow, namely Lax's shock tube problem, the simulation of galloping instabilities of planar detonations and self-similar CJ detonations, with simple chemistry. Lastly, we will investigate galloping detonation instabilities with a realistic hydrogen-oxygen chemical model.

4.1 Lax's shock tube problem

Let us first show the behaviour of the numerical methods for an inert flow. We consider Lax's shock tube problem [23]. Using a fixed reference state, the initial conditions are given as:

$$\begin{cases} p = 3.582\ , \quad T = 7.928\ , \quad u = 0.698 & \text{if } x < 0.5\ , \\ p = 0.571\ , \quad T = 1.142\ , \quad u = 0 & \text{if } x > 0.5\ . \end{cases} \tag{28}$$

The specific heats ratio γ is equal to 1.4. The initial discontinuity splits into a rarefaction wave, a contact discontinuity and a shock wave, and the exact self-similar solution can be easily computed.

For the numerical results presented here, a set of 100 equally spaced nodes is used in the interval $[0, 1]$, with a CFL number of 0.5. Here and in all calculations below, the small parameter δ in the entropy correction (15) is taken equal to 10^{-7}.

The density and pressure profiles obtained at time $t = 0.4$ on a fixed grid and with the MG method are shown on Figure 4, together with the exact solution. We used the MG method with $N_r = 5$ and $N_l = 5$, 10 or 15, but the numerical results were insensitive to our choice of N_l among these three values. Also, the results obtained with the SAG method are almost indistinguishable from those of the MG method: both moving grid methods perfectly resolve the shock wave, whereas the captured shock wave is spread over four mesh points when the TVD method operates on a fixed grid. Notice that we applied the moving mesh strategies only to the shock, and not to the contact discontinuity: this is why the latter remains smeared by the numerical diffusion in all cases on Figure 4.

4.2 Galloping instabilities of one-dimensional detonations

Let us now investigate the problem of longitudinal detonation instability, with the simple one-step chemical model described in Section 2. Choosing the pre-shock state as the reference state, following Fickett and Davis [13], we take the following values of the non-dimensional parameters:

$$\gamma = 1.2\ , \quad Q = 50\ , \quad \beta = 50\ . \tag{29}$$

The longitudinal detonation instability was first shown by Erpenbeck [12]. It was found that the propagating detonation becomes unstable when the overdrive degree f of a strong detonation is smaller than some critical value. For the above parameters (29), the critical value given by Lee and Stewart [24] is $f^c = 1.73$, which is obtained by resolving a system of linearised ODE equations: the propagating detonations are stable for all values of f larger than f^c, and

unstable for all values of f smaller than f^c; in the unstable case, oscillations of the type of a Hopf bifurcation appear. This test-case has been used in several works [1, 4, 5, 8], which we can use to validate our numerical results.

In the computations reported below, the corresponding steady ZND detonation structure is used as the initial condition; the perturbation generated by the truncation error of the numerical method is large enough to lead to the physical instability. Since we are interested in the intrinsic regular oscillation of the detonation front, we prescribe the steady solution at the rear boundary: the piston effect which may cause irregular oscillations is thus eliminated in our simulations. Instead of directly simulating the whole flow driven by the piston, we take a computational domain whose length is thirty times the half-reaction length $L_{1/2}$ of the corresponding steady ZND detonation, and which continually sweeps in order to follow the detonation front; our experiments have shown that this type of reduction of the computational domain does not influence the results, provided that the boundaries, where we add and eliminate mesh points, are far enough from the detonation front. As the taken computational domain is relatively small, a local refinement procedure is not needed and we simply use a set of initially equally spaced mesh points. For the MG method. we take 51 points moving with the front ($N_l = 40$, $N_r = 10$). The CFL number is taken equal to 0.5.

4.2.1 Stable detonations

Let us first consider a stable propagation case, with $f = 1.8$. Figures 5 to 7 show the the history of the Neumann spike pressure obtained on a fixed grid and with the MG and SAG methods. Three spatial resolutions are used: $\Delta x = L_{1/2}/2$, $L_{1/2}/5$ and $L_{1/2}/10$. For the sake of comparison, the exact solution of the corresponding steady ZND detonation is also shown in these figures. Due to the truncation error of the numerical method, oscillations first appear and then damp out with time.

The detonations simulated with the three algorithms are all stable. The long-time pressure obtained on a fixed grid is slightly smaller than the exact value (with a five percent error on the coarsest mesh): this is a consequence of the numerical diffusion, which again spreads the leading shock over four mesh points. With the MG method, the leading shock is always maintained to one cell, and the obtained pressure at the Neumann spike corresponds very well with the exact solution, even on the coarsest mesh. The solutions obtained with the SAG method on the two fine grids are in good agreement with the exact solution; however, the long-time pressure is about two percent larger than the exact value on the coarse mesh. We therefore see that the MG method seem to give better results than the SAG method; this advantage of the MG method over the SAG technique is probably due to the fact that the MG method keeps a uniformly meshed region in the neighbourhood of the shock wave.

4.2.2 Unstable detonations

Next, we consider an unstable propagation case with $f = 1.6$. Figures 8 to 10 show the numerical solutions obtained by the same three algorithms, and with the same three spatial resolutions: $\Delta x = L_{1/2}/2$, $L_{1/2}/5$ and $L_{1/2}/10$.

On the coarsest mesh, the detonation front obtained on a fixed grid is stable, the dynamical

behaviour of the front is not correctly described. As the mesh size is decreased, oscillations appear, and their period is close to 8 times the half-reaction time, in good agreement with the existing results [1, 4, 5, 13]. However, due to the numerical diffusion, the maximum pressure obtained on a fixed grid with $\Delta x = L_{1/2}/5$ is about ten percent smaller than that obtained by the MG method with the same mesh spacing. On the finest mesh, this numerical error is decreased to four percent. The MG produces very good results: its results with $\Delta x = L_{1/2}/5$ are much better than those obtained on a fixed grid with $\Delta x = L_{1/2}/10$. It is also very interesting to notice that the MG method on the coarsest grid already shows the instability, with a period very close to the exact period. Lastly, the SAG method produces very good results on the two fine meshes, but fails to show the instability on the coarsest mesh, where a nonphysical stable behaviour is obtained.

We can conclude here that the MG method improves very much the quality of the numerical results, with in particular a very fine resolution of the Neumann spike. The results produces by our simple MG method are equally good as the results obtained by Bourlioux *et al.* [5] with a more complex shock tracking algorithm. On fine enough mesh, the SAG method also improves a lot the quality of the resolution of the detonation front.

Let us add that, on an even coarser mesh with $\Delta x = L_{1/2}$, none of the algorithms gives acceptable results. The fact that the simulations cannot correctly represent the physical time-dependent behaviour of these unstable detonations when the mesh size is larger than or equal to the half-reaction length can be easily understood on the basis of the following consideration: it is known that the instability results from the interaction between the sound waves, the leading shock wave and the chemical reaction, and that the most unstable acoustic wavelength is typically of the order of the half-reaction length; on a too coarse grid, such waves are very poorly resolved and highly damped, so that the simulations cannot produce correct results.

4.2.3 At the stability threshold

Lastly, we examine the performance of the algorithms for simulations near the stability limit. Figure 11 shows the numerical results obtained with the MG method, for $f = 1.76$, 1.74 and 1.72, using 10 points in the half-reaction length. For $f = 1.76$, the amplitude of oscillations due to the initiation damps out with time and the propagating detonation is stable after time $t = 40$. For $f = 1.74$, the amplitude of oscillations damps very slowly with time and the propagating detonation is also stable. While for $f = 1.72$, the amplitude of oscillations slowly increases with time and the propagating detonation is unstable. The resulting critical value is about $f^c = 1.73$, in perfect agreement with that reported by Lee and Stewart [24].

It seems that, for computations near the instability limit, the developed MG algorithm behaves better than the combination of PPM method with front tracking used by Bourlioux *et al.* [5]: these authors have to use a very fine mesh with $\Delta x = L_{1/2}/20$ in order to get the stability limit f^c; on the mesh with $\Delta x = L_{1/2}/10$, oscillations appear again after $t = 100$ on their numerical solution for $f = 1.76$.

Figure 12 shows the corresponding numerical results obtained with the SAG method on the same mesh. We can see that, for $f = 1.76$, the amplitude of the oscillations becomes very small at $t = 100$, the propagating detonation is stable. On the opposite, the observed detonation is unstable for $f = 1.72$. However, for $f = 1.74$, it is difficult to know from the numerical result whether the propagating detonation is stable or not. Using a very fine mesh with $\Delta x = L_{1/2}/20$,

the result obtained by the SAG method shows that the detonation is stable. These observations show that this simple SAG algorithm behaves as well as the PPM method with front tracking used in [5].

4.3 Self-similar solutions

We now consider a different physical situation. When a detonation wave departs from a fixed closed end of a tube, the propagating detonation is a CJ detonation (for the stable case) followed by a time-dependent rarefaction wave. Neglecting the thickness of the detonation front, one can obtain analytically the spatial distribution of velocity and pressure as a self-similar solution. This is the situation which we now investigate.

For such simulations, the use of a non uniform grid is required to overcome the problem of spatial stiffness, since the boundary of the computational domain is to coincide with the fixed end of the tube. We will employ the MG method combined with local mesh refinement. A finely gridded region is placed around the detonation front and a coarse grid is placed elsewhere; medium-sized meshes are introduced between these two types of grids in order to avoid a brutal variation of the mesh size. The ratio of the coarse and fine grid sizes may vary from 1 to 50. The fine grid and the moderate grids move with the front of the shock wave, following the principle of the MG method.

Choosing a reactive mixture at room temperature (300 K) and ambient pressure (1 atm.) as the reference state, we assume that the non-dimensional parameters now take the values:

$$\gamma = 1.4 \ , \quad Q = 20 \ , \quad \beta = 40 \ . \tag{30}$$

When these parameters are fixed, the stability of the detonation depends on the temperature T_0 of the reactive mixture ahead of the leading shock wave. We consider first a case of stable propagation, with $T_0 = 2$. The length of the computational domain is 1000 times the half-reaction length. The fine cell size is $L_{1/2}/10$, and the fine cells cover a domain of ten times the half-reaction length, moving with the detonation front. The calculation starts from an approximate self-similar solution consisting of a steady CJ detonation followed by a rarefaction wave. The calculated pressure and velocity profiles at $t = 218$, shown on Figure 13, are in very good agreement with the analytical self-similar solutions.

Decreasing the temperature T_0, we may also observe the longitudinal instability of the unsupported CJ detonation. A series of computations have been carried out by varying the temperature T_0, and the results are shown on Figure 14 for $T_0 = 1.4$, 1.5 and 2.0. The stability limit given by these numerical results lies between $T_0 = 1.4$ and $T_0 = 1.5$.

These observations rise the problem of knowing whether the stability of this type of unsupported detonation is the same as that of the *supported* CJ detonation. The same computations have been done using the same spatial resolutions for the supported CJ detonations, and the results are shown on Figure 15 for the same values of T_0. Comparing these results with those shown in Figure 14, we see that the difference of the dynamical behaviours between the supported CJ detonations and the unsupported CJ detonations is very small. The detonation stability appears to depend intrinsically on the detonation front itself.

4.4 Galloping instability in an hydrogen-oxygen mixture

Lastly, we show the result of a simulation of a detonation propagating in an hydrogen-oxygen mixture. The physical model now involves a complete chemical mechanism for the hydrogen-oxygen combustion, with 8 species and 37 reactions; thermodynamical data, such as the values of the specific heats of each species as a function of temperature, are taken from the CHEMKIN package [20]. We consider overdriven detonations propagating in a stoechiometric mixture at atmospheric pressure and ambient temperature (300 K).

In our numerical experiments, the computational domain has a few centimeters in length, and 500 mesh points, among which 200 fine meshes around the front (the fine mesh size is 1.5 10^{-4} cm, so that more than 10 nodes are located within the detonation front). We use the Roe matrix proposed by Shuen *et al.* [30] for the non-perfect gaseous mixture.

In these conditions, the propagation speed of the CJ detonation is 2900 m/s. We have simulated three overdriven detonations with speeds 3100, 3300 and 3600 m/s respectively, using the SAG method. The results are shown on Figure 16, which shows that the two fastest detonation waves are stable, whereas the detonation propagating at 3100 m/s is unstable. These calculations involving complex chemistry are of course much more expensive than those of Section 4.2: one of them takes 5 hours on a SUN Sparc 10 workstation.

5 CONCLUSIONS

We have described a simple but efficient numerical method operating on a moving grid for the simulation of time-dependent planar detonation waves. Detailed comparisons reveal that, for the same spatial resolution, our method behaves as well as (or in some cases even better than) the more complex method of Bourlioux *et al.* [5], which involves a shock tracking technique. In particular, our simple method allowed us to simulate stable and unstable detonations propagating in an hydrogen-oxygen mixture, with detailed thermodynamics and chemistry, which is, to the best of our knowledge, the very first simulation of detonations involving complex chemistry.

Our method is therefore a very good candidate for further computations of planar detonations (and such simulations are for instance needed in order to investigate reduced chemical mechanisms which are appropriate for detonations). Besides, it remains to investigate how our moving grid method could be extended to two space dimensions, to see whether it could be applied to the simulation of non planar detonations.

Let us also add a word on the comparison of our methods with the front tracking method in terms of CPU time. For the shock tube problem, the moving grid methods are about 15% faster than the front tracking technique on a scalar machine (but this advantage may well be more important on a vector computer). However, when realistic chemistry is involved, solving the chemistry takes around 90% of the whole CPU time, so that the differences between the various methods almost vanish.

ACKNOWLEDGEMENTS: This work was supported by DRET under contract 90-103.

References

[1] G. E. Abousieff & T. Y. Toong, Comb. Flame, **45**, p. 67, (1982).

[2] M. Ben-Artzi, J. Comp. Phys., **86**, p. 187, (1990).

[3] J. P. Boris & D. L. Book, J. Comp. Phys. **23**, p. 38, (1973).

[4] A. Bourlioux, *Numerical study of unstable detonation*, PhD Thesis, Princeton University, (1991).

[5] A. Bourlioux, A. Majda & V. Royburd, SIAM J. Appl. Math., **51**, p. 303, (1991).

[6] I. Chern & P. Collela, *A conservative front-tracking method for hyperbolic conservation laws*, Preprint UCRL-97200, Lawrence Berkeley National Laboratory, (1987).

[7] A. Chorin, J. Comp. Phys., **22**, p. 517, (1976).

[8] P. Colella, A. Majda & V. Roytburd, SIAM J. Sci. Stat. Comput., **7**, p. 1059, (1986).

[9] P. Colella & P. Woodward, J. Comp. Phys., **54**, p. 174, (1984).

[10] S. F. Davis, ICASE Report 84-20, Hampton VA, (1984).

[11] W. Döring, Ann. Phys., **43**, p. 421, (1943).

[12] J. J. Erpenbeck, *Theory of detonation stability*, Twelfth Symposium on Combustion (International), The Combustion Institute, p. 711, (1967).

[13] N. Fickett & W. C. Davis, *Detonation*, University of California Press, Berkeley, (1979).

[14] A. Harten, J. Comp. Phys., **49**, p. 357, (1983).

[15] A. Harten, SIAM J. Numer. Anal., **21**, p. 1, (1984).

[16] A. Harten, B. Engquist, S. Osher & S. R. Chakravarthy, J. Comp. Phys., **71**, p. 231, (1987).

[17] A. Harten & J. M. Hyman, J. Comp. Phys., **49**, p. 357, (1983).

[18] L.T. He, PhD thesis, Université de Provence, Marseille, (1991).

[19] L.T. He & P. Clavin, *Critical conditions of detonation initiation in cold reactive gaseous mixtures by nonuniform hot pockets of reactive gases*, Twenty-fourth Symposium on Combustion (International), The Combustion Institute, p. 1861, (1992).

[20] R. J. Kee, J. A. Miller & T. H. Jefferson. *CHEMKIN: a general purpose, problem-independent, transportable, FORTRAN chemical kinetics code package*, SANDIA Report SAND83-8209, (1983).

[21] B. Larrouturou, SIAM J. Sci. Stat. Comput., **10**, p. 742, (1989).

[22] B. Larrouturou, J. Comp. Phys., **95**, p. 59, (1991).

[23] P. D. Lax, Comm. Pure Appl. Math., **7**, p. 159, (1954).

[24] H. I. Lee & D. S. Stewart, J. Fluid Mech., **216**, p. 103, (1990).

[25] R. J. LeVeque & H.C. Yee, J. Comp. Phys., **86**, p. 187, (1990).

[26] D. K. Mao, J. Comp. Phys., **92**, p. 422, (1991).

[27] E. S. Oran & J. P. Boris, *Numerical simulation of reactive flow*, Elsevier, New York, (1987).

[28] P. L. Roe, J. Comp. Phys. **43**, p. 357, (1981).

[29] P. L. Roe, Ann. Rev. Fluid Mech., **18**, p. 337, (1986).

[30] J. S. Shuen, M. S. Liou & B. Van Leer, J. Comp. Phys., **90**, p. 371, (1990).

[31] B. Van Leer, J. Comp. Phys., **23**, p. 263, (1977).

[32] J. Von Neumann, Office of Scientific Research and Development Report 241, p. 549, (1942).

[33] H. C. Yee, Int. J. Comp. Math. Appl., **12**, p. 413, (1986).

[34] H. C. Yee, J. Comp. Phys., **68**, p. 151, (1987).

[35] H. C. Yee, *A class of high-resolution explicit shock capturing methods*, Lecture Notes in Computational Fluid Dynamics, von Karman Institute, (1989).

[36] Y. B. Zeldovich, J. Exp. Theor. Phys., **10**, p. 542, (1940).

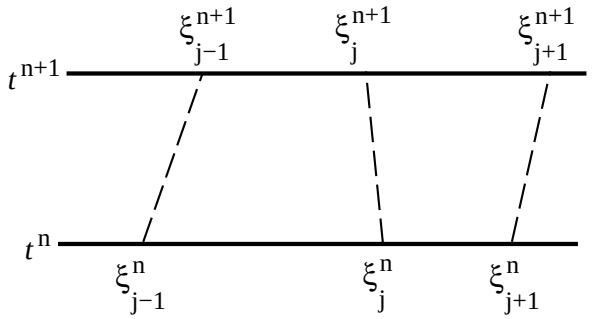

Figure 1: The general moving grid method.

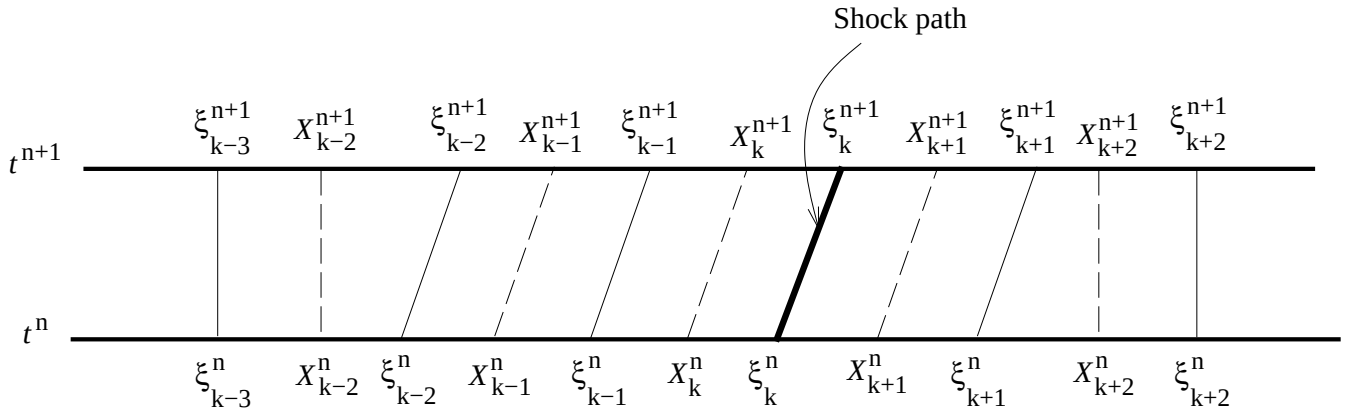

Figure 2: The MG method with $N_l = N_r = 1$.

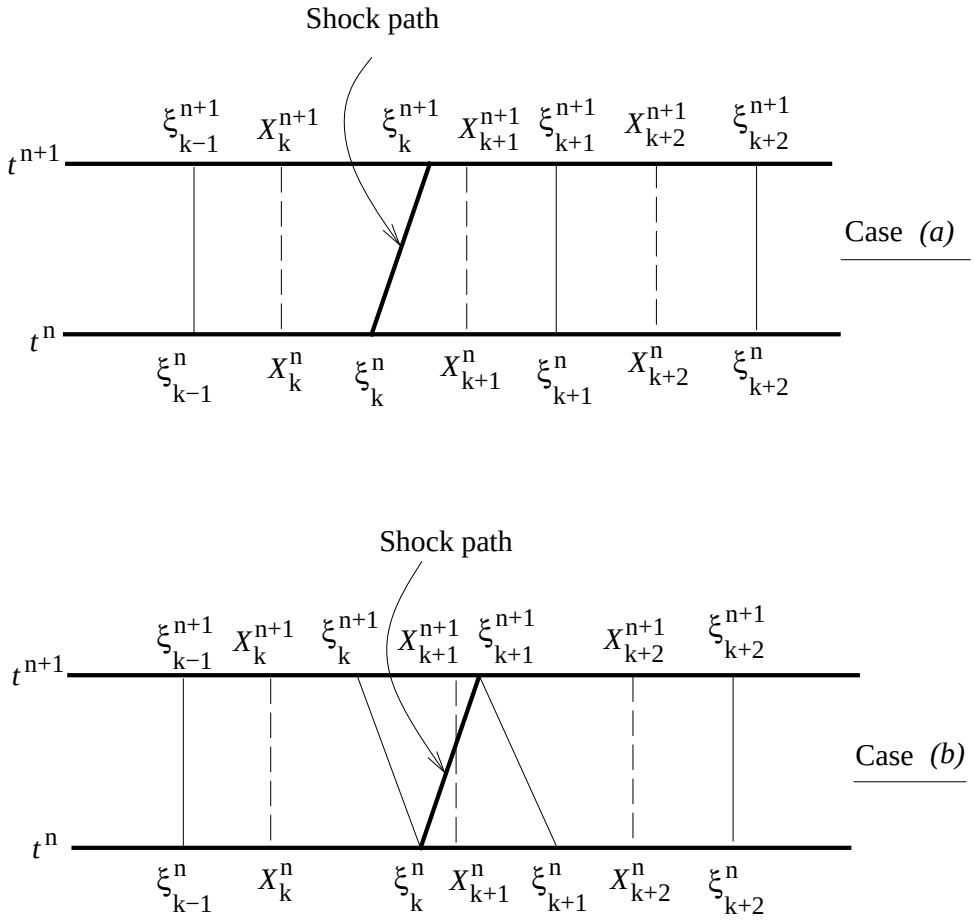

Figure 3: The SAG method.

Figure 4: Density and pressure profiles for Lax's shock tube problem, on a fixed grid (top) and with the MG or SAG methods (bottom).

Figure 5: Pressure at the Neumann spike as a function of time for a stable detonation, with 2, 5 or 10 mesh points per half-reaction length on a fixed grid.

Figure 6: Pressure at the Neumann spike as a function of time for a stable detonation, with 2, 5 or 10 mesh points per half-reaction length using the MG method.

Figure 7: Pressure at the Neumann spike as a function of time for a stable detonation, with 2, 5 or 10 mesh points per half-reaction length using the SAG method.

Figure 8: Pressure at the Neumann spike as a function of time for an unstable detonation, with 2, 5 or 10 mesh points per half-reaction length on a fixed grid.

Figure 9: Pressure at the Neumann spike as a function of time for an unstable detonation, with 2, 5 or 10 mesh points per half-reaction length using the MG method.

Figure 10: Pressure at the Neumann spike as a function of time for an unstable detonation, with 2, 5 or 10 mesh points per half-reaction length using the SAG method.

Figure 11: Pressure at the Neumann spike as a function of time for three values of the overdrive parameter in the neighbourhood of the stability threshold, using the MG method.

Figure 12: Pressure at the Neumann spike as a function of time for three values of the overdrive parameter in the neighbourhood of the stability threshold, using the SAG method.

Figure 13: Pressure and velocity profiles for unsupported detonations.

Figure 14: Pressure at the Neumann spike as a function of time for unsupported detonations, with three different values of the unburnt temperature T_0.

Figure 15: Pressure at the Neumann spike as a function of time for supported detonations, with three different values of the unburnt temperature T_0.

Figure 16: Pressure at the Neumann spike as a function of time for overdriven detonations in an hydrogen-oxygen mixture.